



室蘭工業大学

学術資源アーカイブ

Muroran Institute of Technology Academic Resources Archive



Study on Crosstalk-Free Polarization Splitter Based on Square Lattice Single-Polarization Photonic Crystal Fibers

メタデータ	言語: eng 出版者: IEEE 公開日: 2016-11-29 キーワード (Ja): キーワード (En): wavelength dependence, Square lattice photonic crystal fiber, single polarization transmission, crosstalk-free polarization splitter, finite element method, structural tolerance 作成者: ZHONG, Zheng, ZHANG, Zejun, 辻, 寧英, 江口, 真史 メールアドレス: 所属:
URL	http://hdl.handle.net/10258/00009066

Study on Crosstalk-Free Polarization Splitter Based on Square Lattice Single Polarization Photonic Crystal Fibers

Zheng Zhong, *Student Member, IEEE*, Zejun Zhang, *Student Member, IEEE*,
Yasuhide Tsuji, *Member, IEEE* and Masashi Eguchi, *Member, IEEE*

Abstract—We propose a novel L-shaped crosstalk-free polarization splitter (PS) based on square lattice single polarization photonic crystal fibers (SP-PCFs), which has a wide bandwidth (250 nm) for single polarization transmission. By employing a vectorial finite element method (VFEM) and finite element beam propagation method (FE-BPM), the numerical simulations demonstrate that an incident light polarized in any direction can be split into two orthogonal single polarization states (x - and y -polarizations) without any crosstalk through the proposed PS. Furthermore, a large structural tolerance and a wide transmission bandwidth are also demonstrated, which would lead to more easier fabrication process.

Index Terms—Square lattice photonic crystal fiber, single polarization transmission, crosstalk-free polarization splitter, finite element method, structural tolerance, wavelength dependence.

I. INTRODUCTION

With the development of technology and the rapid popularization of the Internet, higher speed and larger capacity optical communication systems are needed for providing higher quality services of the telecommunication in recent years. Photonic crystal fibers (PCFs) [1], [2], which are treated as an important component of the optical communication systems, are investigated in view of their unique properties of light guidance. PCFs are characterized by a single material with periodically arranged air holes around the core. The guidance mechanism of PCFs is generally classified into two types: total internal reflection and photonic band gap. Therefore, the category of PCFs is always classified into holey fibers (HFs) [3], [4] and photonic band gap fibers (PBGFs) [5], respectively. Unlike conventional step-index fibers, many excellent properties can be achieved easily by the flexible structures of PCF, such as single polarization transmission, endlessly single mode, large birefringence, high nonlinearity, and so on [6]- [9]. Furthermore, single polarization PCFs (SP-PCFs) with various periodic lattices [9]- [11], such as triangular, rectangular, and square lattices, are currently focusing the most attention. By selecting different lattice structures, the desired properties of PCFs can be also achieved.

Polarization splitters (PSs) [12]- [18], which can split an arbitrarily polarized light beam into two orthogonally po-

larized beams, are an important application in the optical communication systems, such as coherent and polarization diversity optical detection. In the past decade, PSs designed by using PCFs have been intensively reported in the world. The operation principle of these PSs reported in [12]- [16] is using the difference of coupling length between x - and y -polarizations. In 2006, Rosa *et al.* proposed a PS based on a kind of square lattice PCF with three cores, which has a device length of 20 mm and an extinction ratio (ER) as low as -23 dB with a bandwidth of 90 nm [15]. After that, Chen *et al.* proposed a PS based on an asymmetric dual-core square-lattice PCF, which has a device length of 5.99 mm and an ER as low as -20 dB with a bandwidth of 101 nm [16]. However, both PSs have relative long device lengths, and the crosstalk between polarization channels. To realize crosstalk-free PSs, Zhang *et al.* firstly presented a crosstalk-free PS with a shorter device length of 1940 μm , a coupling efficiency better than 99% at 1.55 μm , and a wide bandwidth of 160 nm in 2014 [18]. Although it has an excellent polarization split performance in the ideal structure, but the use of elliptical-hole core circular-hole holey fibers (EC-CHF) makes the fabrication of PSs complex. Moreover, the PS has a high possibility to degrade the coupling efficiency, when a minor deviation of the elliptical air holes in the core region occurs. Thus a high precision fabrication technique is required for the practical challenge. And the scattering loss due to the air/silica boundaries in the core may also become a significant issue, since the EC-CHF has air holes in the core. Considering on these points and by employing the SP-PCF without any air holes in the core region, we propose a novel L-shaped crosstalk-free PS based on square lattice SP-PCFs, having only large perfect circular air holes. The reason why we propose a novel L-shaped PS is that, if we choose a horizontal alignment of SP-PCFs like the alignment of EC-CHF in [18], a large coupling length difference between x - and y -polarizations will be caused by the large air holes next to the core. Due to the symmetry of square lattice, the coupling lengths of x - and y -polarizations are the same, and this makes the design procedure of the proposed PS simplified.

In this paper, our goal is to design a novel PS, which can split an incident light polarized in any direction into two orthogonally polarized states without any crosstalk in a wider transmission bandwidth and a higher structural tolerance for practical applications. Firstly, we design and investigate the performances of the SP-PCF and polarization independent-

Z. Zhong, Z. Zhang and Y. Tsuji are with the Division of Information and Electronic Engineering, Muroran Institute of Technology, Muroran, 050-8585 Japan (e-mail:15043030,12054072,y-tsuji@mmm.muroran-it.ac.jp).

M. Eguchi is with the Department of Opto-Electronic System Engineering, Chitose Institute of Science and Technology, Chitose, 066-8655, Japan (e-mail:megu@ieee.org).

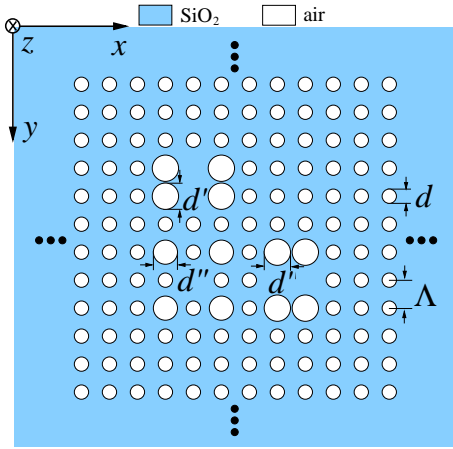


Fig. 1. Cross section of the L-shaped PS with square lattice.

PCF (PI-PCF), which are the main components of the proposed PS. Next, we investigate the performance, structural tolerance, and wavelength dependence of the proposed PS in detail. Finally, we give the conclusion of our study. In all numerical analyses and simulations, we employ the vectorial finite element method (VFEM) [19] to calculate the modal effective indices of waveguides, and the light propagation behavior in the proposed PS is simulated by using the vectorial finite element beam propagation method (FE-BPM) [20].

II. STRUCTURE OF THE PROPOSED PS

In this section, we investigate a novel L-shaped PS, shown in Fig. 1. It has three cores consisting of a PI-PCF in the middle and two SP-PCFs in the upper and right side, respectively. The PS is characterized by a single material of SiO₂ and the holes are filled by air. Here, the centers of all air holes are arranged with the lattice pitch of Λ , the diameter of the cladding air hole is represented by d . The diameters of larger air holes, which are adjacent to the core regions of the SP-PCFs and the PI-PCF, are represented by d' and d'' , respectively. In order to achieve the crosstalk-free PS with a low insertion loss and wider operation bandwidth, first, we design an SP-PCF to broaden its operation bandwidth. Next, a PI-PCF is designed to satisfy the perfect phase matching condition with the SP-PCFs. Under this design procedure and according to the mode coupling theory, we believe that the maximum of coupling efficiency of the PS can be achieved, which means that the respective x - and y -polarized lights can be outputted without any crosstalk from the corresponding SP-PCF core ports.

A. Design of the SP-PCFs

We consider a single-polarization single-mode PCF [9] with a square lattice to guide a single-polarized light. Due to the symmetry of square lattice, once either the x - or y -polarized SP-PCF structure is designed, the other polarized SP-PCF structure can be obtained by rotating the prior structure in 90 degrees. This nature simplifies the design procedure of the PS. Here, we only investigate the performance of x -polarized SP-PCF, which is referred to as x SP-PCF and shown in Fig.

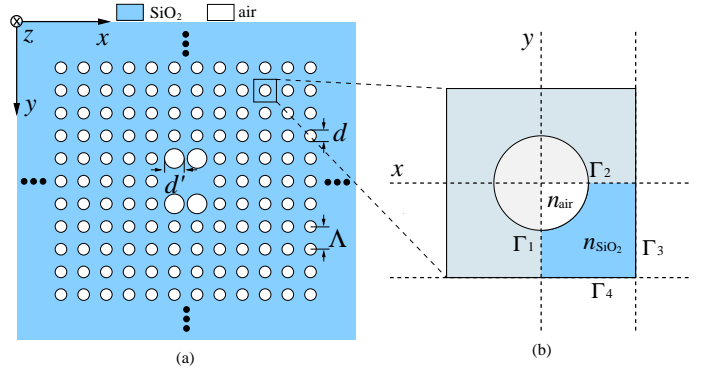


Fig. 2. Cross section of the x SP-PCF (a) and the unit cell of square lattice (b). The quarter bright region in (b) is an elementary piece and the boundary pairs $[\Gamma_1, \Gamma_3]$ and $[\Gamma_2, \Gamma_4]$ are paired for loading the perfect electric conductor (PEC) or perfect magnetic conductor (PMC).

2(a). By enlarging the four air holes over and under the core, the anisotropic geometry in the x and y directions has been realized. Since the cutoff wavelengths of x - and y -polarized modes of the x SP-PCF are different, the single polarization transmission can be achieved in these SP-PCFs. In [21], Mägi *et al.* have demonstrated the tapering of a photonic crystal holey fiber to achieve a microstructure pitch of less than 300 nm by using the post-processing technique and the flame brushing technique. That means a lattice pitch smaller than $\sim 2 \mu\text{m}$ can be realized. Therefore, in order to achieve the single polarization transmission in the communication wavelength band, we select a lattice pitch Λ of $1.2 \mu\text{m}$ and the cladding air hole diameter d of 0.51Λ . The refractive indices of SiO₂ and air are set to be $n_{\text{SiO}_2} = 1.45$ and $n_{\text{air}} = 1$, respectively. The infinite number of the cladding air hole rings is assumed, because if the number of air hole rings is finite, the confinement loss must be considered. However, in our PS the device length is very short, the confinement loss can be almost negligible. Meanwhile, we do not take into account the material dispersion either, because the device length of the proposed PS is shorter than 1 mm. Under these settings, we employ the VFEM to estimate the single polarization transmission bandwidth against the air hole diameter d' , which is shown in Fig. 3. The light blue region represents the non-confinement region, where the modal effective index of either x - or y -polarization is smaller than the effective index of the fundamental space-filling mode (FSM). FSM of a PCF is defined as a mode with the largest modal index of the infinite 2-D photonic crystal constituted in the cladding region of a PCF [22]. In order to simplify the calculation, we just apply the VFEM to the elementary piece (bright region in Fig. 2(b)), which is a quarter of the unit cell of square lattice, to calculate the modal effective index of the FSM. That is because there is structural symmetries along the x - and y -axes (illustrated by dashed lines) in the unit cell. The schematic drawing of the unit cell is shown in Fig. 2(b). And there are two boundary pairs along the symmetric plane. For the x -polarized mode, PEC and PMC are applied to the boundary pairs $[\Gamma_1, \Gamma_3]$ and $[\Gamma_2, \Gamma_4]$, respectively. The modal effective indices of x - and y -polarizations are illustrated by the solid line and the

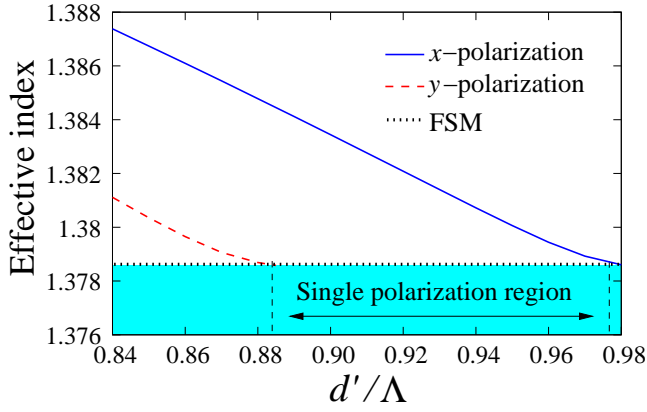


Fig. 3. The modal effective indices of x - and y -polarizations and the FSM as a function of normalized air hole diameter d'/Λ .

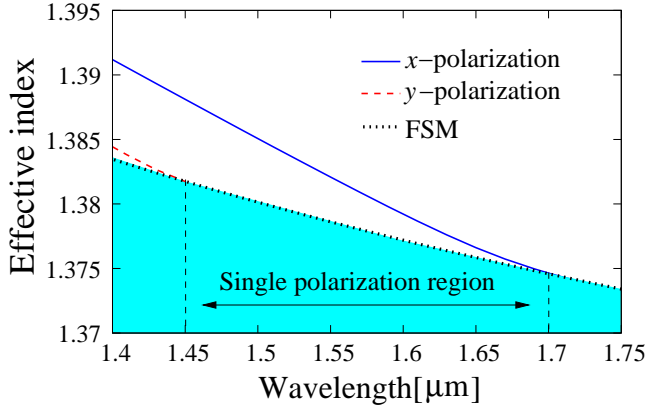


Fig. 4. The modal effective indices of x - and y -polarizations and the FSM as a function of wavelength. The condition of air hole size $d' = 0.92\Lambda$ with $\Lambda = 1.2 \mu\text{m}$ is determined to obtain a wideband of 250 nm single polarization transmission.

dashed line, respectively. It can be seen that, when the air hole diameter d' is selected in the range from 0.885Λ to 0.976Λ , the single polarization transmission can be achieved. Here, we determine $d' = 0.92\Lambda$ to obtain sufficiently wideband single polarization transmission at the operating wavelength of $1.55 \mu\text{m}$. At that time, The modal effective indices of x - and y -polarized modes and the FSM as a function of wavelength is shown in Fig. 4. When the wavelength is in the range of 1.45 to $1.70 \mu\text{m}$, the modal effective index of y -polarized mode is lower than that of the FSM and the cutoff wavelength of y -polarized mode is shorter than that of x -polarized mode. It is demonstrated that only the x -polarized mode can be guided sufficiently in the x SP-PCF.

B. Design of the PI-PCF

As an incident PCF port, a PI-PCF is used for guiding both x - and y -polarizations, and in order to satisfy the perfect phase matching condition with the SP-PCFs, the design of the air holes around the core of PI-PCF is required. Therefore, we enlarge the four air holes at the corners of the core region to destroy the symmetric core geometry. Although enlarging all the air holes around the core is possible, but the coupling with the adjacent SP-PCFs will be weak, which then leads to

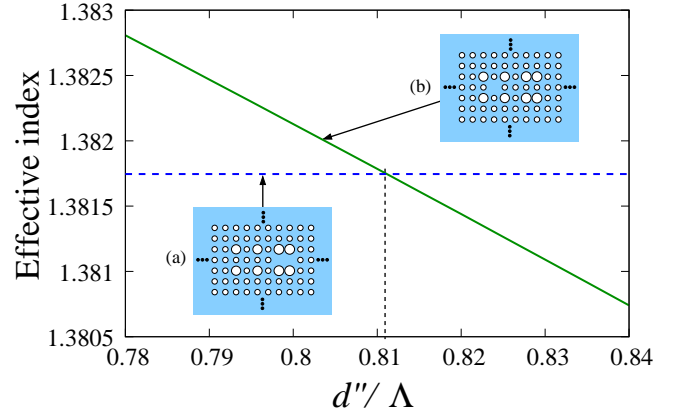


Fig. 5. The modal effective indices of x -polarizations of x MSP-PCF and MPI-PCF as a function of normalized air hole diameter d''/Λ ; the insert (a) and (b) show the cross section of x MSP-PCF and MPI-PCF, respectively.

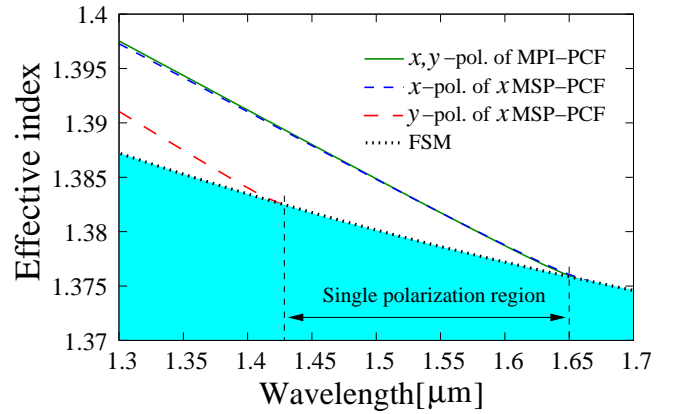


Fig. 6. The modal effective indices of x - and y -polarizations of x MSP-PCF and MPI-PCF and the FSM as a function of wavelength. A bandwidth of 220 nm of the single polarization transmission is achieved under the condition of $\Lambda = 1.2 \mu\text{m}$, $d' = 0.92\Lambda$, $d'' = 0.8112\Lambda$.

longer device length. Thus, we just enlarge four air holes at the corners to make the coupling with the SP-PCFs strong. At the first, we calculate the modal effective indices of the isolated fiber cores (x SP-PCF and PI-PCF) separately. However, in the coupling system the contribution of the large air holes between adjacent fiber cores must be concerned. Thus, we redesign the SP-PCF and the PI-PCF in the same coupling system. By defecting the core of x SP-PCF into the cladding air holes, which means the large air holes around the core of x SP-PCF are also regarded as the cladding air holes. The structure designed in this way is defined as the modified PI-PCF (MPI-PCF) in the isolated system. Under the same procedure, the modified SP-PCFs (MSP-PCF) can be also obtained. Here, we calculate the modal effective indices of the x MSP-PCF and MPI-PCF to determine the parameter d'' . The modal effective indices as a function of normalized air hole diameter d''/Λ is shown in Fig. 5, and the operating wavelength is set to $\lambda = 1.55 \mu\text{m}$. The modal effective index of MPI-PCF is illustrated by the solid line, and the effective index of x MSP-PCF is illustrated by the dashed line. Moreover, the inserts (a) and (b) also show the cross sections of x MSP-PCF and MPI-PCF, respectively. The cross point of the dashed and the solid

lines means that the perfect phase matching condition between x MSP-PCF and MPI-PCF is satisfied, where the diameter of four air holes at the corners of the PI-PCF core region is $d'' = 0.8112\Lambda$. At the same time, the modal dispersion curves of these PCFs as a function of wavelength are shown in Fig. 6, which illustrate the modal effective indices of the MPI-PCF, x - and y -polarized modes of x MSP-PCF and FSM, respectively. We can find that two orthogonal polarized modes are independent in the MPI-PCF and only x -polarized mode can be transmitted through the x MSP-PCF with a bandwidth of 220 nm ($1.43 \mu\text{m} \sim 1.65 \mu\text{m}$). Compared with the isolated x SP-PCF discussed in Section A, the bandwidth of single polarization transmission is shifted to the short wavelength side and is narrowed to 30 nm. Therefore, it is obvious that the contribution of the large air holes between adjacent waveguides is significant and must be concerned.

III. ANALYSIS OF THE PS WITH SP-PCFs

In this section, firstly, we present that all the structural parameters of the proposed PS depend on the previous design of the SP-PCFs and the PI-PCF. Next, we numerically analyze the PS to obtain the effective indices of even and odd modes by employing the VFEM. Finally, when a 45-degree polarized light beam is inputted, we simulate the light propagation behavior in the PS by employing the FE-BPM.

We set the PS structure shown in Fig. 1 as the initial structure, the materials of the PS are pure silica (SiO_2) and air, and we assume the refractive indices of SiO_2 and air to be $n_{\text{SiO}_2} = 1.45$ and $n_{\text{air}} = 1$, respectively. When the perfect phase matching condition is satisfied between the adjacent cores, the diameters of holes in each part are set to be $d = 0.51\Lambda$, $d' = 0.92\Lambda$, and $d'' = 0.8112\Lambda$ with the lattice pitch $\Lambda = 1.2 \mu\text{m}$, the operating wavelength is set to $\lambda = 1.55 \mu\text{m}$. Table I shows the effective indices of even and odd modes and the estimated coupling lengths for the x - and y -polarizations, respectively. Here, the coupling length L_c is calculated by the mode coupling theory, which can be defined by

$$L_c = \frac{0.5\lambda}{n_{\text{eff,e}} - n_{\text{eff,o}}}, \quad (1)$$

where λ is the operating wavelength, $n_{\text{eff,e}}$ and $n_{\text{eff,o}}$ are the effective indices of even and odd modes, respectively, in the coupled system. The same coupling lengths of x - and y -polarizations, which are equal to $695 \mu\text{m}$, are demonstrated. Therefore, the device length L can be shortened to $695 \mu\text{m}$. Based on these conditions, the simulation of light propagation behavior in the PS along the propagation direction z is also demonstrated as shown in Fig. 7, where the longitudinal step Δz is set to $1 \mu\text{m}$, the analyzed region is $27.0 \times 27.0 \mu\text{m}^2$, and the total unknowns are 821,578 in this analysis. We can observe that, with the light propagation, a 45-degree polarized incident light inputted into PI-PCF can be split the x - and y -polarized mode components to the x SP- and y SP-PCF cores, respectively, completely and the crosstalk-free is firmly of strictly guaranteed along the propagation. At that time, the normalized power evolution as a function of z is also

TABLE I
EFFECTIVE INDICES OF EVEN AND ODD MODES AND THE ESTIMATED COUPLING LENGTHS OF THE PS

	Effective index		Coupling length
	Even mode	Odd mode	L_c [μm]
x -pol.	1.382274	1.381159	695
y -pol.	1.382274	1.381159	695

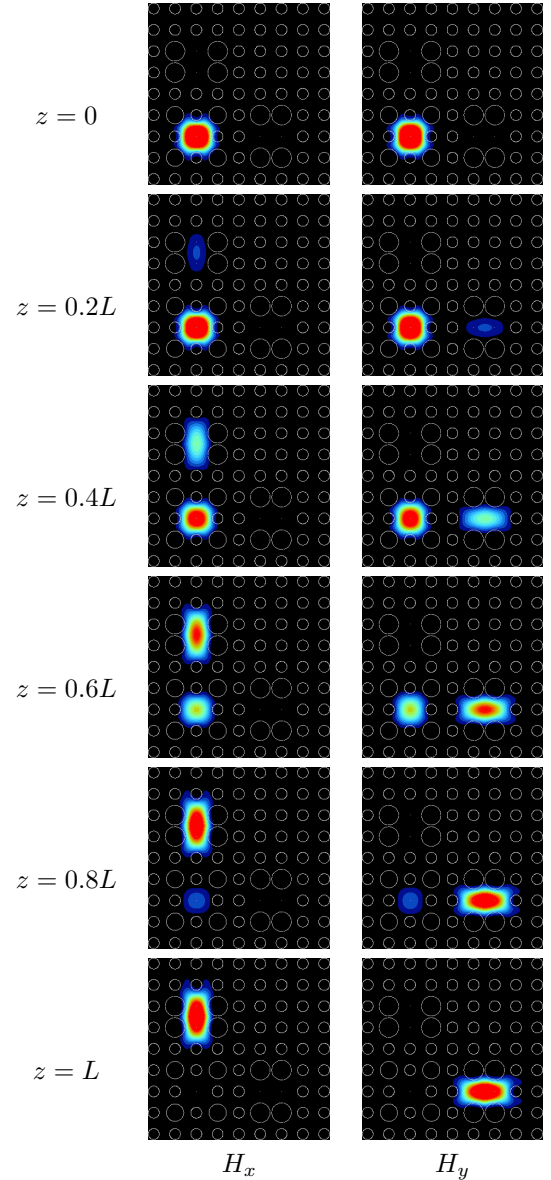


Fig. 7. Light propagation behavior in the proposed PS along the propagation distance z , H_x and H_y are the magnetic field distribution of y - and x -polarization, respectively. Since x - and y -polarization only couples with corresponding x SP- and y SP-PCF, crosstalk free is guaranteed in the propagation.

estimated, as shown in Fig. 8. The coupling efficiency F is defined by

$$F = 1 - \left(\frac{n_{\text{eff},1} - n_{\text{eff},2}}{n_{\text{eff,e}} - n_{\text{eff,o}}} \right)^2, \quad (2)$$

where $n_{\text{eff},1}$ and $n_{\text{eff},2}$ are the effective indices of the isolated

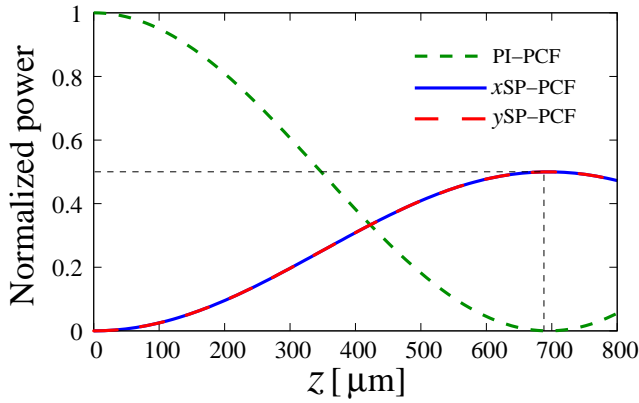


Fig. 8. Normalized power evolution as a function of propagation distance z .

waveguides [18]. In this paper, these effective indices are shown in Fig. 5 in Section II. Under this condition, the normalized powers represented by NP of PI-PCF and SP-PCF are given by

$$NP_{(\text{SP-PCF})} = \frac{F}{2} \sin^2 \left(\frac{\pi}{2L} z \right), \quad (3)$$

$$NP_{(\text{PI-PCF})} = 1 - \frac{F}{2} \sin^2 \left(\frac{\pi}{2L} z \right). \quad (4)$$

It is demonstrated that, at the propagation distance $z = 695 \mu\text{m}$, 100% of the incident light of the PI-PCF can be split half and half into the x SP- and y SP-PCFs without any crosstalk.

IV. TOLERANCE AND WAVELENGTH DEPENDENCE OF PS

In order to confirm whether the PS can be fabricated easily under the current fabrication technology, we need to estimate the performance of PS on the structural tolerance. In [23], it has been reported that the fabrication accuracy of circular air holes in the PCFs could be controlled within $\pm 1\%$. Under the same circumstance and considering the various uncertain factors in the process of fabrication, we calculate the coupling efficiency of PS, when the large air holes around the core in only one waveguide (y SP-PCF, PI-PCF, or x SP-PCF) or the cladding are deviated at the same level. Or in another words, we deviate only one parameter of the air hole diameters d , d' of x SP-PCF, d'' of y SP-PCF, and d''' at a time within $\pm 1\%$. It can be seen in Table II that, with all the results estimated with percentage, the worst coupling efficiency of PS reduced to approximately 87.2%, and the hole deviations of x SP- and y SP-PCFs lead to almost the same degradations of the coupling efficiency. Meanwhile, the hole deviations of PI-PCF and the cladding can keep the coupling efficiency more than 93.8%. However, by estimating the fabrication errors from percentage to nanometer, in the fabrication error range of $\pm 11 \text{ nm}$, the proposed PS can realize the same performance with the PS consisting of EC-CHFs having small holes in the fabrication error range of only $\pm 3.7 \text{ nm}$ in [18]. Moreover, we also make a discussion on the coupling efficiency variation of the PS with the condition of all air holes deviated randomly in the range of $\pm 1\%$ simultaneously. Fig. 9 shows the coupling efficiency of PS as a function of the deviation of hole radius.

TABLE II
COUPLING EFFICIENCY VERSUS THE DEVIATION FOR DIFFERENT PARTS OF THE DEVICE PARAMETERS AT EACH DEVIATION LEVEL

Deviation level	Core region			Cladding region
	y SP-PCF	PI-PCF	x SP-PCF	
-1.0%	87.4%	94.3%	87.2%	96.1%
-0.5%	96.1%	98.5%	96.0%	98.9%
-0.4%	97.4%	99.0%	97.4%	99.3%
-0.3%	98.5%	99.5%	98.5%	99.6%
0%	100%	100%	100%	100%
0.3%	98.5%	99.4%	98.5%	99.5%
0.4%	97.4%	99.0%	97.4%	99.2%
0.5%	96.2%	98.4%	96.2%	98.7%
1.0%	87.5%	93.8%	87.5%	94.8%

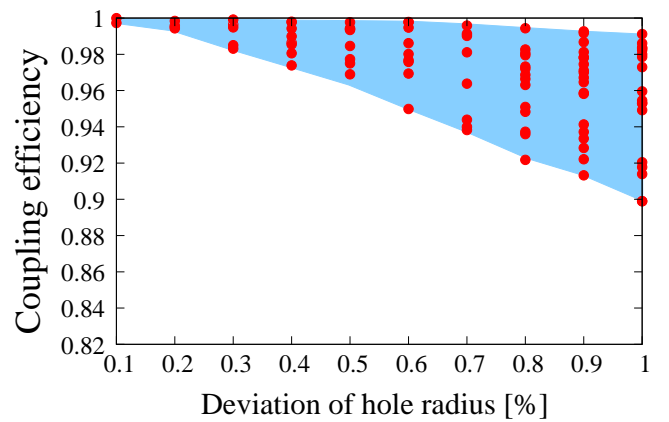


Fig. 9. Coupling efficiency variation versus the random deviation of all holes radii within $\pm 1\%$.

The light blue region shows the deviation range of the coupling efficiency. Within the deviation range of $0.1\% \sim 1\%$, the coupling efficiency is decreased. Even in the worst case, the coupling efficiency can still be kept at about 90%. Hence, a larger structural tolerance can be realized in the PS with SP-PCFs and the problem, that the effective index is sensitive to the air holes in the core region of the EC-CHFs in [18], is solved as well.

One more important performance, the wavelength dependence of PS, is also required to be estimated for the wideband transmission in the optical communication systems. Under the condition of the single polarization transmission bandwidth of the SP-PCF designed in Section II, we investigate the wavelength dependence of the proposed PS in the single polarization wavelength range of $1.43 \mu\text{m}$ to $1.65 \mu\text{m}$, which is shown in Fig. 10. Firstly, we investigate the wavelength dependence of the PS designed at a wavelength of $1.55 \mu\text{m}$, which is shown by the solid line. The coupling efficiency better than 99% can be achieved from $1.46 \mu\text{m}$ to $1.62 \mu\text{m}$, where the transmission bandwidth is the same as the PS consisting of small hole EC-CHFs of 160 nm in [18]. However, since the cutoff wavelength of odd mode is shorter than that of the isolated system, the operating band is restricted to wavelengths shorter than $1.62 \mu\text{m}$. Thus, this transmission bandwidth can

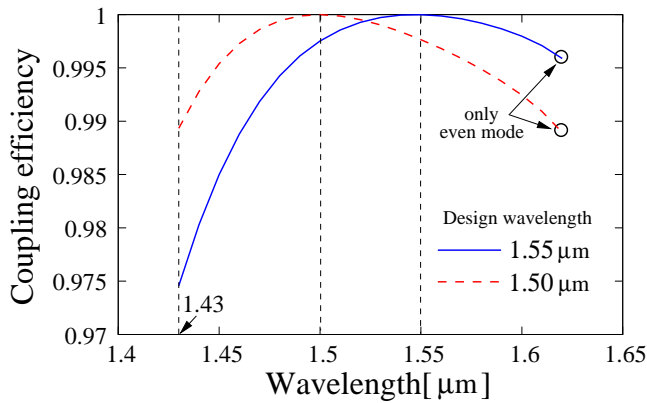


Fig. 10. Wavelength dependence of the proposed PS at different design wavelength. The solid and dashed lines show the coupling efficiencies at the design wavelength of $1.55 \mu\text{m}$ and $1.50 \mu\text{m}$, respectively. The places denoted by open circles represent the cutoff wavelength of the odd mode.

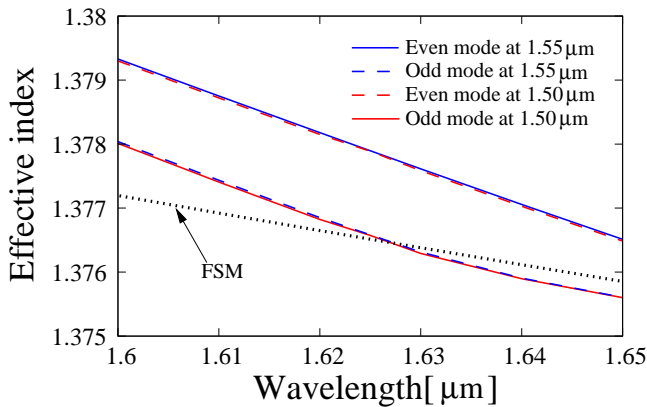


Fig. 11. The modal effective indices of even and odd modes of the PS designed at different wavelength and the FSM as a function of wavelength. When the wavelength is longer than $1.62 \mu\text{m}$ in both cases, the odd mode is already cut off by the FSM.

not cover the single polarization transmission bandwidth of SP-PCF. Hence, we try to shift the design wavelength from 1.55 to $1.50 \mu\text{m}$ to earn a wider bandwidth by adjusting the air hole sizes of the PI-PCF core region from $d'' = 0.8112\lambda$ to 0.8127λ , with the condition of that the size of air holes around the SP-PCF core is unchanged. At that time, the perfect phase matching condition between the adjacent cores is satisfied at the design wavelength of $1.50 \mu\text{m}$. The result is shown by the dashed line in Fig. 10. Under this procedure, the transmission bandwidth can be broadened to 180 nm with the coupling efficiency better than 99% , where the wavelength is from $1.431 \mu\text{m}$ to $1.611 \mu\text{m}$. However, when the wavelength is longer than $1.62 \mu\text{m}$ in both cases, only the even mode can be transmitted, because the odd mode is already cut off by the FSM. At that time the dispersion curves of even and odd modes and FSM are shown in Fig. 11. It can be seen that even if d'' is changed from 0.8112λ to 0.8127λ , the cutoff wavelength of odd mode is not changed and the coupling efficiency does not droop too much. Only the central wavelength, satisfying perfect phase matching, is shifted. We should note that no matter how the structural deviation occurs, the crosstalk-free is still guaranteed by the single polarization

nature of the SP-PCFs in Table II and Fig. 9.

V. CONCLUSION

In this paper, we proposed a novel three core L-shaped polarization splitter based on square lattice single polarization photonic crystal fibers, which can split incident light polarized in any direction into two orthogonally polarized waves without any crosstalk. We use the SP-PCFs with large perfect air holes to replace the EC-CHF used in [18], in order to solve the precision problem in manufacturing elliptical air holes. And the advanced performances of the PS are demonstrated in detail. A higher structural tolerance and a wider transmission bandwidth are also demonstrated in the proposed PS. Combined with the existing techniques such as the stack and draw technique, post-processing technique, flame brushing technique, interlaced stacking technique and so on, we believe that the proposed PS can be fabricated and applied for the practical applications.

REFERENCES

- [1] J. C. Knight, T. A. Birks, P. St. J. Russell, and D. M. Atkin, "All-silica single-mode optical fiber with photonic crystal cladding," *Opt. Lett.*, vol. 21, issue 19, pp. 1547–1549, Oct. 1996.
- [2] P. St. J. Russell, "Photonic-crystal fibers," *J. Lightw. Technol.*, vol. 24, no. 12, pp. 4729–4749, Dec. 2006.
- [3] M. Eguchi and Y. Tsuji, "Single-mode single-polarization holey fiber using anisotropic fundamental space-filling mode," *Opt. Lett.*, vol. 32, no. 15, pp. 2112–2114, Aug. 2007.
- [4] K. Ichikawa, Z. Zhang, Y. Tsuji, and M. Eguchi, "A single-polarization holey fiber with anisotropic lattice of circular air holes," *J. Lightw. Technol.*, vol. 33, no. 18, pp. 3866–3871, Sep. 2015.
- [5] M. Eguchi and Y. Tsuji, "Single-polarization elliptical-hole lattice core photonic-bandgap fiber," *J. Lightw. Technol.*, vol. 31, no. 1, pp. 177–182, Jan. 2013.
- [6] T. A. Birks, J. C. Knight, and P. St. J. Russell, "Endlessly single-mode photonic crystal fiber," *Opt. Lett.*, vol. 22, no. 13, pp. 961–963, Jul. 1997.
- [7] J. Ju, W. Jin, and M. Suleyman Demokan, "Design of single-polarization single-mode photonic crystal fiber at 1.30 and $1.55 \mu\text{m}$," *J. Lightw. Technol.*, vol. 24, no. 2, pp. 825–830, Feb. 2006.
- [8] M. Sharma, N. Borogohain, and S. Konar, "Index guiding photonic crystal fibers with large birefringence and walk-off," *J. Lightw. Technol.*, vol. 31, no. 21, pp. 3339–3344, Nov. 2013.
- [9] K. Saitoh and M. Koshiba, "Single-polarization single-mode photonic crystal fibers," *IEEE Photon. Technol. Lett.*, vol. 15, no. 10, pp. 1384–1386, Oct. 2003.
- [10] F. Zhang, M. Zhang, X. Liu, and P. Ye, "Design of wideband single-polarization single-mode photonic crystal fiber," *J. Lightw. Technol.*, vol. 25, no. 5, pp. 1184–1189, May 2007.
- [11] M. Chen, B. Sun, and Y. Zhang, "Broadband single-polarization operation in square-lattice photonic crystal fibers," *J. Lightw. Technol.*, vol. 28, no. 10, pp. 1443–1446, May 2010.
- [12] L. Zhang and C. Yang, "Polarization splitter based on photonic crystal fibers," *Opt. Exp.*, vol. 11, no. 9, pp. 1015–1020, May 2003.
- [13] K. Saitoh, Y. Sato, and M. Koshiba, "Polarization splitter in three-core photonic crystal fibers," *Opt. Exp.*, vol. 12, no. 17, pp. 3940–3946, Aug. 2004.
- [14] L. Zhang and C. Yang, "Polarization-dependent coupling in twin-core photonic crystal fibers," *J. Lightw. Technol.*, vol. 22, no. 5, pp. 1367–1373, May 2004.
- [15] L. Rosa, F. Poli, M. Foroni, A. Cucinotta, and S. Selli, "Polarization splitter based on a square-lattice photonic-crystal fiber," *Opt. Lett.*, vol. 31, no. 4, pp. 441–443, Feb. 2006.
- [16] M. Chen, B. Sun, Y. Zhang, and X. Fu, "Design of broadband polarization splitter based on partial coupling in square-lattice photonic-crystal fiber," *Appl. Opt.*, vol. 49, no. 16, pp. 3042–3048, Jun. 2010.
- [17] Z. Zhang, Y. Tsuji, and M. Eguchi, "Design of polarization splitter with single-polarization elliptical-hole core circular-hole holey fibers," *IEEE Photon. Technol. Lett.*, vol. 26, no. 6, pp. 541–543, Mar. 2014.

- [18] Z. Zhang, Y. Tsuji, and M. Eguchi, "Study on crosstalk-free polarization splitter with elliptical-hole circular-hole holey fibers," *J. Lightw. Technol.*, vol. 32, no. 23, pp. 3956–3962, Dec. 2014.
- [19] M. Koshihara and Y. Tsuji, "Curvilinear hybrid edge/nodal elements with triangular shape for guided-wave problems," *J. Lightw. Technol.*, vol. 18, no. 4, pp. 737–743, May 2000.
- [20] Y. Tsuji and M. Koshihara, "Adaptive mesh generation for full-vectorial guided-mode and beam-propagation solutions," *IEEE J. Sel. Topics Quantum Electron.*, vol. 6, no. 1, pp. 163–169, Jan. /Fed. 2000.
- [21] E. C. Mägi, P. Steinvurzel, and B. J. Eggleton, "Tapered photonic crystal fibers," *Opt. Exp.*, vol. 12, no. 5, pp. 776–784, Mar. 2004.
- [22] Y. Li, C. Wang, Y. Chen, M. Hu, B. Liu, and L. Chai, "Solution of the fundamental space-filling mode of photonic crystal fibers: numerical method versus analytical approaches," *Appl. Phys. B*, vol. 85, pp. 597–601, May 2006.
- [23] S. Lou, Z. Tang, and L. Wang, "Design and optimization of broadband and polarization-insensitive dual-core photonic crystal fiber coupler," *Appl. Opt.*, vol. 50, no. 14, pp. 2016–2023, May 2011.



Zheng Zhong (S'15) was born in Yantai, Shandong, China, on June 26, 1989. He received the B.S. degree in Department of Information and Electronic Engineering from Muroran Institute of Technology, Muroran, Japan, in 2015.

He is a Student Member of the Institute of Electronics, Information and Communication Engineers (IEICE).



Zejun Zhang (S'14) was born in Jiaozuo, Henan, China, on April 3, 1989. He received the B.S. degree in Department of Electrical Engineering from Xuchang University, Xuchang, Henan, China, in 2011, and he received the M.S. degree in Division of Information and Electronic Engineering from Muroran Institute of Technology, Muroran, Japan, in 2014.

He is a Student Member of the Institute of Electronics, Information and Communication Engineers (IEICE).



Yasuhide Tsuji (M'97) was born in Takikawa, Japan, on December 31, 1967. He received the B.S., M.S., and Ph.D. degrees in electronic engineering from Hokkaido University, Sapporo, Japan, in 1991, 1993, and 1996, respectively.

In 1996, he joined the Department of Applied Electronic Engineering, Hokkaido Institute of Technology, Sapporo, Japan. From 1997 to 2004, he was an Associate Professor of Electronics and Information Engineering at Hokkaido University. From 2004 to 2011, he was an Associate Professor of Electrical

and Electronic Engineering at Kitami Institute of Technology, Kitami, Japan. Since 2011, He is a Professor of Division of Information and Electronic Engineering at Muroran Institute of Technology, Muroran, Japan. He has been engaged in research on optical wave electronics.

Dr. Tsuji is a Member of the Institute of Electronics, Information and Communication Engineers (IEICE), the Japan Society of Applied Physics, the Optical Society of America (OSA). In 1997, 1999, and 2015, he was awarded the Excellent Paper Award from IEICE. In 2000, he has received the Third Millennium Medal from IEEE.



Masashi Eguchi (M'93) was born in Sapporo, Japan, on August 9, 1962. He received the B.S. degree in electronic engineering from Kitami Institute of Technology, Kitami, in 1985 and the M.S. and Ph.D. degrees in electronic engineering from Hokkaido University, Sapporo, Japan, in 1987, 1991, respectively.

He joined Sony Co., Ltd., in 1987. From 1991 to 1995, he was with the Department of Industrial Design, Sapporo School of the Arts, Sapporo, Japan. And from 1995 to 1998, he was an Associate Professor of Center for Multimedia Aided Education Educational Center for Information Processing at Muroran Institute of Technology, Muroran, Japan. Since 1998, He is an Associate Professor of the Faculty of Department of Opto-Electronic System Engineering, Chitose Institute of Science and Technology, Chitose, Japan. He has been engaged in research on various optical fibers, dielectric waveguides, optical solitons, and applications of finite element method and other electromagnetic wave analysis methods.

Dr. Eguchi is a Senior Member of the Optical Society of America (OSA) and a Member of the Institute of Electronics, Information and Communication Engineers (IEICE).